2011 IEEE/RSJ International Conference on
Intelligent Robots and Systems
September 25-30, 2011. San Francisco, CA, USA

Three Module Lumped Element Model of a Continuum Arm Section

N. Giri, I. D. Walker, *Fellow, IEEE*

Abstract— **In this paper, a section of a continuum arm is modeled using lumped model elements (masses, springs and dampers). The model, although an approximation for a continuum structure, can be used to conveniently analyze the dynamics of the arm with selectable tradeoff in accuracy of modeling. Principles of lagrangian dynamics are used to derive the expressions for the generalized forces in the system. Simulation results using the model are compared with the physical measurements of a continuum arm prototype built using McKibben actuators. A brief discussion on how this relatively simple model can be more realizable when compared to other techniques of modeling continuum arms is also presented in the paper.**

I. Introduction

CONTINUUM robots represent a class of robots that have a bio-inspired form characterized by flexible backbones and high degrees of freedom structures [1]. Such robots have potential applications in whole arm grasping and manipulation in unstructured environments such as rescue operations. For a detailed description of robots built that resemble biological trunk, tentacles and tongue, see [2],[3],[4],[5] and [6]. Theoretically, the compliant nature of a continuum robot provides infinite degrees of freedom to these devices. However, there is a limitation set by the practical inability to incorporate infinite actuators in the device. Most of these robots are consequently underactuated, or in other words they can achieve a wide range of configurations with relatively few control inputs. For example, the Octarm VI continuum manipulator (figure 1) has nine independent degrees of freedom with only three sections.

Continuum manipulators differ fundamentally from rigid link and hyper-redundant robots by having an unconventional structure that lacks links and joints. Hence, standard techniques like the Denavit-Hartenberg (D-H) algorithm cannot be directly applied for developing continuum arm kinematics. Moreover, the design of each continuum arm varies w.r.t the flexible backbone present in the system, the positioning, type and number of actuators. The constraints imposed by these factors make the set of reachable configurations and nature of movements unique to every continuum robot. This makes it difficult to formulate generalized kinematic or dynamic models for continuum robot hardware. Chirikjian and Burdick were the first to introduce a method for modeling the kinematics of a continuum structure by representing the curve-shaping function using modal functions [7]. Mochiyama used Serret-Frenet formulae to develop kinematics of hyper-degrees of freedom manipulator [8]. For details on the more manipulator-specific kinematics of the Rice/Clemson "Elephant trunk" manipulator, see [9],[10],[11]. For the Air Octor and Octarm continuum robots, more general forward and inverse kinematics have been developed by incorporating the transformations of each section of the manipulator (using D-H parameters of an equivalent virtual rigid link robot) and expressing those in terms of the continuum manipulator section parameters [12]. The net result of the work in [7]-[12] is the establishment of a general set of kinematic algorithms for continuum robots.

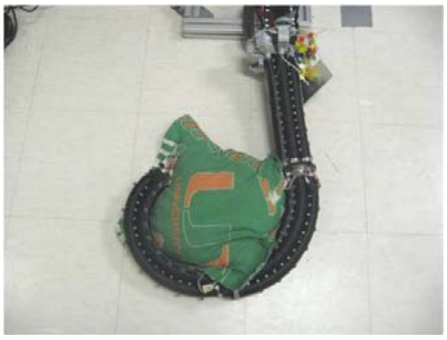

Fig. 1. Octarm VI continuum manipulator

Thus, the kinematics of a few prototypes of continuum manipulators has been developed and basic control strategies now exist based on these. Recently, the development of analytical models to analyze continuum arm dynamics is actively being focused on by several researchers in this field. The first approach to this was proposed by Chirikjian, based on an infinite degree of freedom model [13]. In [14], Newton Euler equations along with a Cosserat beam model were used to model the dynamics of an eel-like robot. Later, 3D position tracking and motion control with feedback for the eel-like robot were developed [15]. Also based on Cosserat theory of elastic rods, a non-closed form, geometrically exact model was developed in [16]. A novel method of modeling planar motion of snake-like robots using virtual work principles and by the addition of a nominal mechanism to snake-like

Manuscript received March14, 2011. This work was supported in part by the U.S. national Science Foundation Grant IIS-0844954 and IIS-0904116.

The authors, N. Giri and I. D. Walker are with the Department of Electrical and Computer Engineering, Clemson University, Clemson, SC 29634. (e-mail: ngiri@clemson.edu; iwalker@clemson.edu).

robot body is presented in [17]. A detailed account of closed-form Lagrangian dynamic models for continuum robots is covered in [18], [19] and [20]. Tatlicioglu's work ([19] and [20]) extended the model developed by Mochiyama and Suzuki for Continuum Robots that have extensibility as an additional degree of freedom. However, the fundamental approach of modeling full continuum arm dynamics based on classical or continuum mechanics is not favorable due to the magnitude of complexity involved. There is a pressing need to adopt a completely different modeling scheme or to introduce sufficient assumptions in the model which will make its realization feasible with an acceptable compromise in its accuracy. While Tatlicioglu's work utilized a geometric model of a Continuum Robot, we have used a linearized dynamic model of the actuators as the building blocks of the section's model.

The work illustrated in this paper derives inspiration from modeling of biological segments using discrete mechanical elements [21],[22]. The principal modeling idea is to slice a continuum structure into a finite number of similar modules and represent each module using lumped parameter elements. This model will be seen to be quite effective, at the cost of retention of some complexity issues. Useful features of the approach and issues impeding further development are discussed in later sections of this paper.

II. Dynamic Model-An Overview

This work is primarily intended to study the dynamics of general continuum robots. To ground the results on real hardware, the model herein is focused on the Octarm VI continuum robot [12], [23]. Hence, the parameters and constraints implemented in this model conform to that of Octarm VI. Octarm VI is a three section continuum robot. Each section is made up of three McKibben actuators tied together along their lengths. A section of the device extends when there are equal pressure levels in all three actuators and bends when there are different pressure levels in the actuators (noticing that there is no torsion along the length of the arm). Since each section bends in space to form a constant curvature section its analysis can be restricted to a plane during these movements (the orientation of the plane changes as the robot moves). Therefore, a planar model is effective for the case of a single continuum robot section, the subject of the analysis in this paper. The shape of a section of the continuum arm is parameterized by the variables, s - length of arc, κ - curvature and φ – orientation. In the 2-D single-section case, orientation (φ) can be neglected.

Two actuators are sufficient to model planar operation of a single-section of a continuum arm. We model each actuator as a Mckibben actuator, as realized in the Octarm hardware. Each such pneumatic actuator has air-filled latex tubing enclosed in a braided sleeve. The inherent compliance and damping of the actuator will be represented by a linear spring and damper combination. Thus each module in the model has a pair of linear spring and damper struts. The actuators maintain a nearly constant diameter at all pressure levels and this is accounted for in the model by constraining the distance between the two spring and damper struts. The length of arc (s) of each module is the average length of the two actuators. Another parameter, θ, is introduced to account for bending such that $\frac{1}{\kappa}=\frac{s}{\theta}$.

Fig. 2. Octarm VI, individual actuators and planar equivalent prototype

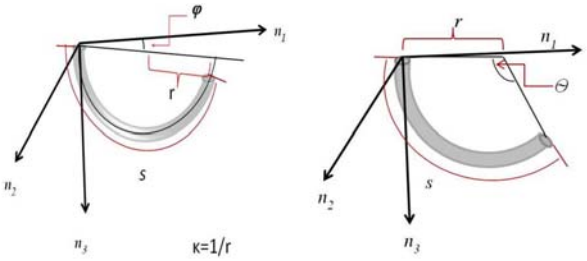

Fig. 3. Parameters in spatial and planar configurations (originally appeared in [23])

III. Derivation of the Three-Module Model

The continuum section analytical model developed here consists of three modules stacked together in series. In general, the model will be a more exact replication of the behavior of a continuum arm with a greater number of modules included in series. However, we will show that three modules effectively represent the dynamic behavior of the hardware, so more complex models are not motivated.

The generalized co-ordinates in the system are,

s_i, θ_i for i=1,2,3

The subscript, i denotes the module number. The

generalized forces corresponding to the generalized co-ordinates are,

Q_{s_i} , Q_{θ_i} for i=1,2,3

There is a generalized force and a generalized torque in the system which imparts a linear velocity and a bending torque respectively. The forces F_{1i}, F_{2i} for i=1,2,3 represent the input forces due to air muscles in the system. Since air-pressure is uniform throughout the entire length of each of the actuators, the corresponding input forces acting in all the three modules should be same. Thus, the constant curvature bend exhibited by the section is incorporated inherently within the model.

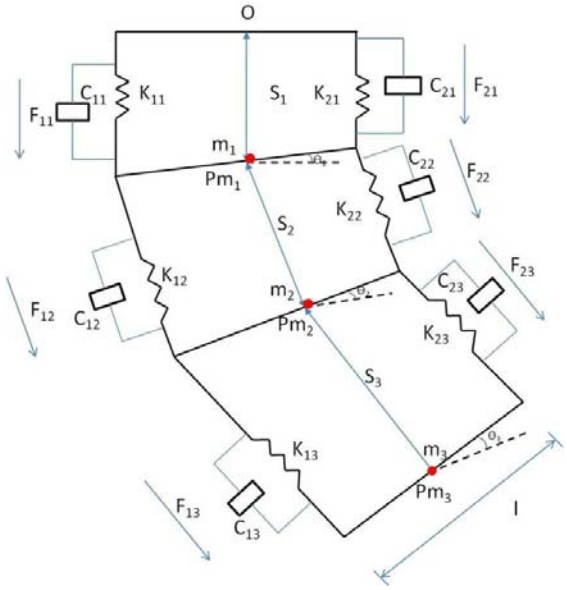

Fig. 4. Analytical Model of a section of a Continuum Arm

The other model parameters are,

l - Length of the rigid rod connecting the two struts

k_{1i}, i=1,2,3 - Spring constant of actuator1

k_{2i}, i=1,2,3 - Spring constant of actuator2

c_{1i}, i=1,2,3 - Damping coefficient of actuator1

c_{2i}, i=1,2,3 - Damping coefficient of actuator2

m_i,i=1,2,3 - Mass in each module

I_i,i=1,2,3 - Moment of inertia of the rigid rod in each module

The mass of the arm is modeled as being concentrated at three points whose co-ordinates referenced w.r.t a global inertial frame (N) located at the base of the arm are given below,

$$^{N}P_{m_1}=s_1\hat{n}_3 \quad (1)$$

$$^{N}P_{m_2}=s_2\sin\theta_1\hat{n}_1+(s_1+s_2\cos\theta_1)\hat{n}_3 \quad (2)$$

$$^{N}P_{m_3}=(s_2\sin\theta_1+s_3\sin(\theta_1+\theta_2))\hat{n}_1+(s_1+s_2\cos\theta_1+s_3\cos(\theta_1+\theta_2))\hat{n}_3 \quad (3)$$

The position vector of each mass is initially defined in a frame local to the module in which it is present. These local frames are located at the base of each module and oriented along the parameter 's' of that module. The rotations and the translations between the local frames and the base frame (located at point O) are given in appendix.

By differentiating the position vectors, we obtain the linear velocities. The kinetic energy(T) of the system comprises of linear kinetic energy terms and rotational kinetic energy terms which are due to rotation of the rigid rod connecting the two actuators.

$$T=(1/2)m_1\dot{s}_1^2+(1/2)m_2((\dot{s}_2\sin\theta_1+s_2\cos\theta_1\dot{\theta}_1)^2+(\dot{s}_1+\dot{s}_2\cos\theta_1-s_2\sin\theta_1\dot{\theta}_1)^2)+(1/2)m_3((\dot{s}_2\sin\theta_1+s_2\cos\theta_1\dot{\theta}_1+\dot{s}_3\sin(\theta_1+\theta_2)+s_3\cos(\theta_1+\theta_2)\dot{\theta}_1+s_3\cos(\theta_1+\theta_2)\dot{\theta}_2)^2+(\dot{s}_1+\dot{s}_2\cos\theta_1-s_2\sin\theta_1\dot{\theta}_1+\dot{s}_3\cos(\theta_1+\theta_2)-s_3\sin(\theta_1+\theta_2)\dot{\theta}_1-s_3\sin(\theta_1+\theta_2)\dot{\theta}_2)^2)+(1/2)I_1\dot{\theta}_1^2+(1/2)I_2(\dot{\theta}_1^2+\dot{\theta}_2^2)+(1/2)I_3(\dot{\theta}_1^2+\dot{\theta}_2^2+\dot{\theta}_3^2) \quad (4)$$

The potential energy (P) of the system is the sum of the gravitational potential energy and the spring energy. A small angle assumption is made throughout the derivation. This allows us to express the displacement of springs and the velocities associated with dampers in terms of the system parameters.

$$P=-m_1gs_1-m_2g(s_1+s_2\cos\theta_1)-m_3g(s_1+s_2\cos\theta_1+s_3\cos(\theta_1+\theta_1))+(1/2)k_{11}(s_1+(l/2)\theta_1-s_{01})^2+(1/2)k_{21}(s_1-(l/2)\theta_1-s_{01})^2+(1/2)k_{12}(s_2+(l/2)\theta_2-s_{02})^2+(1/2)k_{22}(s_2-(l/2)\theta_2-s_{02})^2+(1/2)k_{13}(s_3+(l/2)\theta_3-s_{03})^2+(1/2)k_{23}(s_3-(l/2)\theta_3-s_{03})^2 \quad (5)$$

where, s_{01},s_{02} and s_{03} are the initial values of s_1,s_2 and s_3 respectively.

Due to viscous damping in the system, Rayleigh's dissipation function is given by,

$$D=(1/2)c_{11}(\dot{s}_1+(l/2)\dot{\theta}_1)^2+(1/2)c_{21}(\dot{s}_1-(l/2)\dot{\theta}_1)^2+(1/2)c_{12}(\dot{s}_2+(l/2)\dot{\theta}_2)^2+(1/2)c_{22}(\dot{s}_2-(l/2)\dot{\theta}_2)^2+(1/2)c_{13}(\dot{s}_3+(l/2)\dot{\theta}_3)^2+(1/2)c_{23}(\dot{s}_3-(l/2)\dot{\theta}_3)^2 \quad (6)$$

The generalized forces in the system corresponding to the generalized co-ordinates are expressed as appropriately weighted combinations of the input forces. For details on the derivation, refer to the appendix.

$$Q_{s_1}=F_{11}+F_{21}+(F_{12}+F_{22})\cos\theta_1+(F_{13}+F_{23})\cos(\theta_1+\theta_2) \quad (7)$$

$$Q_{s_2} = F_{12} + F_{22} + (F_{13} + F_{23})\cos(\theta_2) \quad (8)$$

$$Q_{s_3} = F_{13} + F_{23} \quad (9)$$

$$Q_{\theta_1} = (l/2)(F_{11} - F_{21}) + (l/2)(F_{12} - F_{22}) + (l/2)(F_{13} - F_{23}) + s_2 \sin\theta_2 (F_{13} + F_{23}) \quad (10)$$

$$Q_{\theta_2} = (l/2)(F_{12} - F_{22}) + (l/2)(F_{13} - F_{23}) \quad (11)$$

$$Q_{\theta_3} = (l/2)(F_{13} - F_{23}) \quad (12)$$

It can be evinced from the force expressions that the total input forces acting on each module can be resolved into an additive component along the direction of extension and a subtractive component that results in a torque. For the first module, there is an additional torque produced by forces in the third module.

The model resulting from the application of Lagrange's equations of motion obtained for this system can be grouped in the form,

$$F_{coeff}\,\underline{\tau} = D(\underline{q})\ddot{\underline{q}} + C(\underline{q})\dot{\underline{q}} + G(\underline{q}) \quad (13)$$

Where, $\underline{\tau}$ is a vector of input forces and $\underline{q}$ is a vector of generalized co-ordinates. The force coefficient matrix F_{coeff} transforms the input forces to the generalized forces and torques in the system. The inertia matrix, D is composed of four block matrices. The block matrices that correspond to pure linear accelerations and pure angular accelerations in the system (on the top left and on the bottom right) are symmetric. The matrix C contains coefficients of the first order derivatives of the generalized co-ordinates. Since the system is nonlinear, many elements of C contain first order derivatives of the generalized co-ordinates. The remaining terms in the dynamic equations resulting from gravitational potential energies and spring energies are collected in the matrix G. In the following examples, this highly coupled nonlinear system of differential equations is solved numerically using SIMULINK. The problem being moderately stiff, ode23t solver is chosen as the optimum solver. Also, the dynamic plots of the state variables obtained using different solvers were compared with the plot of the explicit solution of the model with equal input forces and it was confirmed that the dynamics obtained using ode23t solver matched the explicit solution.

V. Model Validation and Numerical Results

Having identified the parameters that define the shape of the continuum arm, a simple prototype replicating the dynamics of a single section of the Octarm was built to validate the model. Two McKibben actuators of identical sizes were coupled together along their length. These actuators were assembled by enclosing a high temperature silicon rubber tubing inside a polyester mesh sleeve and one of its ends was sealed with a brass stopper and a brass connecter was fit to the other end that connects to the pressure adapter, thereby to the pressure lines. A compressor was used as a pressure source and the air flow in each of the actuator was regulated by a pressure regulator (ITV3010-01N11L4) that was controlled by an Arduino microcontroller (Arduino Duemilanove with ATMega328). The dimensions of the actuator are tabulated in TABLE I.

The initial displacements (s_{0i}) of all three modules are taken as one-third of the unpressurized muscle length and the initial orientations (θ_{0i}) are taken as 0. Since the variation of mass with increase in air pressure is negligible, we split the value as twice the mass of an unpressurized muscle between the masses in the model. The masses of the terminal modules are made 0.06 Kg heavier than the mass of the second module since the brass connectors at either ends of the actuator constitute 60 % of the actuator weight. The value of l is two times the diameter of the sleeve.

TABLE I
Prototype Dimensions

Parameters of a single actuator	Value
Muscle length (including terminals)	0.5207 m
Muscle length (excluding terminals)	0.3937 m
Muscle diameter	0.0171 m
Mass of the actuator (unpressurized)	0.18 Kg
Variation in mass from 101.6 kPa to 344.737 kPa	1.1%
Inner and outer diameters of silicon tubing	9.5 mm, 12.7 mm
Diameter of the mesh sleeve	12.7 mm

To determine the stiffness constant, the actuator was loaded in steps of 1 pound increments at its lower end (with its upper end clamped) and the corresponding displacements were measured. The force-displacement relationship is approximately linear and the slope of the line fit to the data by least squares method is taken as the value of the stiffness constant. The increase in stiffness with pressure is close to linearity and a least square curve fit is used to calculate the stiffness constant at various actuation levels in the model.

The next important parameter to be characterized was the force F exerted by the muscles. The muscle actuation is intrinsic, the most dominant factors inflicting a change in the force being the pressure level and the braid angle. Chou and Hannaford were the first to derive a force expression for McKibben actuators by modeling the shape of a contractor muscle as a cylinder whose diameter and length are expressed by the parameters of the mesh [25].

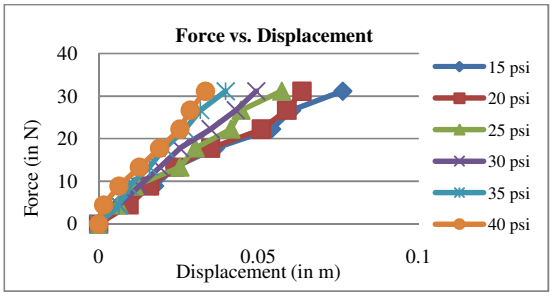

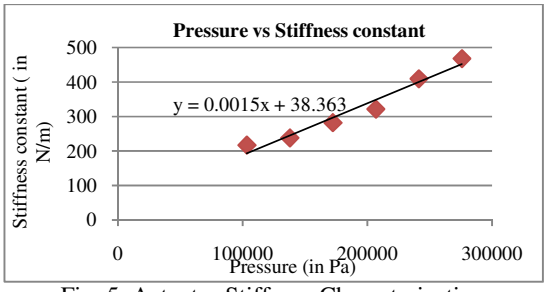

Fig. 5. Actuator Stiffness Characterization

Contractors are air muscles that contract in length and expand in diameter when pressurized. In contrast to this, the extensor muscles considered in this paper and prevalent in continuum robots increase in length at a nearly constant diameter when pressurized. However, since the physical compositions of both the actuators are same, we have followed a similar procedure described in [25] to derive a force-pressure relationship. Employing the concept of virtual work,

$$P_r dV = FdL \quad (14)$$

where P_r is the relative pressure (difference between the actuator pressure and the atmospheric pressure), dV and dL are the changes in volume and length respectively. For an extensor, the diameter is observed to be nearly constant throughout the range of working pressures (from 101.35 kPa to 448.15 kPa). Hence, $dV = \frac{\pi D^2 dL}{4}$, where D is the diameter of the sleeve. Thus the force required to obstruct the extension of the muscle is, $F = \frac{\pi D^2 P_r}{4}$. Theoretically, this force is equally divided between the three modules and the stiffness constant of springs in each module is thrice that of the actuator. To account for the above, we have multiplied the force by 0.1 in each module. The damping coefficients are tuned so that the model is critically damped.

The actuators are set to desired pressure levels by programming the Arduino to send appropriate PWM signals to its analog outputs that are connected to the control inputs of the pressure regulators. The length of the arc was measured by running a thread along the groove formed at the centre by the coupled actuators. The orientation was measured using a protractor. In few cases, images of the prototype were clicked and orientation angles were found using image processing in MATLAB.

The s_i and θ_i of all three modules in the model are summed up to obtain the overall length of arc (s) and orientation (θ) of the arm. The numerical solution for different inputs and the actual values measured on the prototype are tabulated in TABLE II and III.

The first module had the highest displacement (followed by the second and third modules, respectively) in most of simulation cases except for several when gravitational effects were not considered in the system. These were the cases with large pressure difference in the two actuators which caused more bending and hence a decrease in displacement of module one. With gravity included in the system, the orientation angles in the terminal modules were almost the same and greater than that in the second module. However since the displacement decreases from first module to third module, the radius of curvature is almost the same in first and second modules and the third module has more curvature than the other two. This is exactly the shape of the real device, which curls more near the tip with a nearly constant curvature throughout the rest of its structure. Without gravity in the system, the angles decreased from module one to three. This indicates a nearly constant curvature (since the displacements also decrease in the same order) throughout the length of the actuator – this is also observed in the physical model when operated on a horizontal surface.

TABLE II
MEASUREMENTS AND NUMERICAL SOLUTIONS FOR CASES WITH GRAVITY IN THE SYSTEM

Pressure in actuator1 (in kPa)	Pressure in actuator2 (in kPa)	Measured values		Simulation results	
		s (in m)	θ (in degrees)	s (in m)	θ (in degrees)
103.421	103.421	0.405	0	0.418	0
172.362	172.362	0.435	0	0.438	0
310.261	310.261	0.463	0	0.457	0
137.894	103.421	0.425	6.6	0.421	8.9
206.841	103.421	0.430	23	0.431	20.1
344.735	137.894	0.449	26.3	0.447	23.3
344.735	275.788	0.469	3.4	0.457	4.7

TABLE III
MEASUREMENTS AND NUMERICAL SOLUTIONS FOR CASES WITHOUT GRAVITY IN THE SYSTEM

Pressure in actuator1 (in kPa)	Pressure in actuator2 (in kPa)	Measured values		Simulation results	
		s (in m)	θ (in degrees)	s (in m)	θ (in degrees)
103.421	103.421	0.402	0	0.401	0
172.362	172.362	0.432	0	0.426	0
310.261	310.261	0.461	0	0.451	0
137.894	103.421	0.413	52.7	0.404	41.9
206.841	103.421	0.429	84.5	0.398	118
344.735	137.894	0.445	99.9	0.385	212
344.735	275.788	0.468	27	0.447	29.7

From the results, it can be inferred that the overall length of the arm (s) obtained from the model is very close to the values measured from the device. Our orientation measures from the physical device had a considerable error margin and hence it is unclear how well the model fits the device. The large difference in angles in some cases is attributed to the inability of the device to bend more overcoming the friction offered by the horizontal surface. However, since continuum robots are mostly operated in a spatial environment, we conclude that the model gives sufficiently precise information about the overall configuration of the arm. Although the analytical model can be refined by adding more modules, a three module model appears sufficient to give a general sense of the structure of the arm as well as its configuration details.

VI. CONCLUSION

We have introduced a new approach to modeling the dynamics of sections of continuum robots. The approach is based on lumped model elements (masses, springs and dampers). The model, although an approximation for a continuum structure, is seen to conveniently analyze the dynamics of the arm with selectable tradeoff in accuracy of modeling. Simulation results using the model are compared with the physical measurements of a continuum arm prototype built using McKibben actuators. The relatively simple model (compared to other techniques of modeling continuum robots) demonstrates good approximation to the physical situation.

APPENDIX

The rotation matrices between the local frames (l_1,l_2 and l_3) and the base frame (N) are given below,

$$R_{l_1}^{\ N}=\begin{pmatrix}1 & 0 & 0\\ 0 & 1 & 0\\ 0 & 0 & 1\end{pmatrix};\ R_{l_2}^{\ N}=\begin{pmatrix}\cos(\theta_1) & 0 & \sin(\theta_1)\\ 0 & 1 & 0\\ -\sin(\theta_1) & 0 & \cos(\theta_1)\end{pmatrix}$$

$$R_{l_3}^{\ N}=\begin{pmatrix}\cos(\theta_1+\theta_2) & 0 & \sin(\theta_1+\theta_2)\\ 0 & 1 & 0\\ -\sin(\theta_1+\theta_2) & 0 & \cos(\theta_1+\theta_2)\end{pmatrix}$$

The translations are given as follows,

$$T_{l_1}^{\ N}=\begin{pmatrix}0\\ 0\\ 0\end{pmatrix};\ T_{l_2}^{\ N}=\begin{pmatrix}0\\ 0\\ s_1\end{pmatrix};\ T_{l_3}^{\ N}=\begin{pmatrix}s_2\sin\theta_1\\ 0\\ s_1+s_2\cos\theta_1\end{pmatrix}$$

An expression for generalized forces, Q_k in terms of applied forces, F_j for a system having 'p' number of forces and 'n' number of generalized co-ordinates is given below [24],

$$Q_k=\sum_{j=1}^{p}F_j.\frac{\partial \dot{r}_j}{\partial \dot{q}_k},\qquad k=1,2,...,n$$

The points at which the actuator forces act (r_j) are expressed in their respective local frames and then rotated and translated to be referenced in the base inertial frame.

ACKNOWLEDGMENT

This research was supported in part by the U.S. National Science Foundation under grants IIS-0904116 and IIS-1017007.

REFERENCES

[1] G. Robinson, and J. Davies, "Continuum robots – a state of the art,"*Proc. IEEE International Conference on Robotics and Automation*, Detroit, MI, 1999, vol. 4, pp. 2849-2854.

[2] V. C. Anderson, and R. C. Horn, "Tensor arm manipulator design," *ASME*, paper #67-DE-57,1967.

[3] S. Hirose, *Biologically Inspired Robots*, Oxford University Press, 1993.

[4] H. Tsukagoshi, A. Kitagawa, and M. Segawa, "Active hose: an artificial elephant's nose with maneuverability for rescue operation," *Proc. IEEE International Conference on Robotics and Automation (ICRA),* Seoul, Korea, May 2001, pp.2454-2459.

[5] K. Suzumori, S. Iikura, H. Tanaka, "Applying a flexible micro-actuator to robotics mechanics," *IEEE Control Syst. Mag.,* vol.12, pp. 21-26, Feb. 1992.

[6] I. D. Walker, and M. W. Hannan, "A novel elephant's trunk robot," *Proc. IEEE/ASME International Conference on Advanced Intelligent Mechatronics*, Atlanta, GA, Sept. 1999, pp. 410-415,

[7] G. S. Chirikjian, and J. W. Burdick, "A modal approach to hyper-redundant manipulator kinematics," *IEEE Transactions on Robotics and Automation*, vol. 10, No. 3, Jun 1994, pp. 343354.

[8] H. Mochiyama, E. Shimemura, and H. Kobayashi, "Direct kinematics of manipulators with hyper degrees of freedom and serret-frenet formula," *IEEE International Conference on Robotics and Automation*, pp. 1653-1658, 1988.

[9] I. Gravagne, and I. D. Walker, "Kinematic transformations for remotely-actuated planar continuum robots," *IEEE International Conference on Robotics and Automation*, pp. 19-26, 2000.

[10] I. Gravagne, and I. D. Walker, "Kinematics for constrained continuum robot using wavelet decomposition," *Proceedings of the 4th Int. Conf. and Expo./Demo. on Robotics for Challenging Situations and Environments*, pp. 292-298, 2000.

[11] M. W. Hannan, and I. D. Walker, "Kinematics and the implementation of an elephant's trunk manipulator and other continuum style robots," *J. Robotic Syst*., 20(2), 45–63, 2003.

[12] B. A. Jones, and I. D. Walker, "Kinematics for multi-section continuum robots," *IEEE T. Robot*., 22, 1, 43–55, 2006.

[13] G. S. Chirikjian, "Hyper-Redundant manipulator dynamics: a continuum approximation," *Adv. Robot.*, Vol. 9, No. 3, Jun. 1995, pp. 217243.

[14] W. Khalil, G. Gallot, O. Ibrahim and F. Boyer, "Dynamic modeling of a 3-D serial eel-like robot," *Proc. IEEE Int. Conf. Robot. Autom.*, Barcelona, Spain, 2005, pp. 1282-1287.

[15] M. El Rafei, M. Alamir, N. Marchand, M. Porez and F. Boyer," Motion control of a three-dimensional eel-like robot without pectoral fins," *Proc of the 17th IFAC World Congress*, 2008, vol. 17, part 1.

[16] D. Trivedi, A. Lofti and C.D.. Rahn,"Geometrically exact dynamic models for soft robotic manipulators," *IEEE Int. Conf. Intel. Robot. Sys.*, San Diego, CA, 2007, pp. 1497-1502.

[17] N. Li, T. Zhao and Y. Zhao, "The dynamic modeling of snake-like robot by using nominal mechanism method," *Intel. Robot. and Appl.*, Springer–Verlag, Berlin–Heidelberg 2008.

[18] H. H. Mochiyama and T. Suzuki, "Kinematics and dynamics of a cable-like hyper-flexible manipulator," *Proc. IEEE Int. Conf. Robot. Autom.*, Taipei, Taiwan, 2003, pp. 3672-3677.

[19] E. Tatlicioglu, I.D. Walker and D.M. Dawson, "Dynamic modeling for planar extensible continuum robot manipulators," *Int. Jour. Robot. Autom.*, Vol. 24, No. 4, 2009.

[20] E. Tatlicioglu, I.D. Walker and D.M. Dawson, "New dynamic models for planar extensible continuum robot manipulators," *IEEE Int. Conf. Intel. Robot. Sys.*, San Diego, CA, 2007, pp. 1485-1490.

[21] Y. Yekutieli, R. Sagiv-Zohar, R. Aharonov, Y. Engel, B. Hochner and T. Flash, "Dynamic model of the octopus arm I. biomechanics of the octopus arm reaching movement," *Journ. Neurophy.*, vol. 94, 2005, pp. 1443-1458.

[22] E. S. Mallet, G. T. Yamaguchi, J. M. Birch, and K. C. Nishikawa, "Feeding motor patterns in anurans: insights from biomechanical modeling," *Journal of life sciences*, vol. 41, issue 6, pp. 1364-1374.

[23] N. Giri, I. D. Walker, "Continuum robots and underactuated grasping," *Mechanical Sciences*, vol. 2,pp. 51-58.

[24] L. Meirovitch, *Methods of Analytical Dynamics*, McGraw-Hill Book Company, 1970, pp. 46-100.

[25] C. Chou, B. Hannaford, "Measurement and modeling of McKibben pneumatic artificial muscles," *IEEE Transactions on Robotics and Automation*, vol. 12, no. 1, Feb. 1996, pp 90-102.